Subphthalocyanine Semiconducting Cocrystals with Efficient Super-Exchange Coupling

Lingyan Sun,[1] Yuan Guo,*[,2,3] Dan He,[4] Barun Dhara[5], Fei Huang,[1] Yuanping Yi,[3] Daigo Miyajima*[,6] and Cheng Zhang*[,1]

[1]Key Laboratory of Green Chemistry and Technology of Ministry of Education, College of Chemistry, Sichuan University, Chengdu 610064, P. R. China

[2]School of Light Industry and Engineering, Qilu University of Technology (Shandong Academy of Sciences), Jinan 250353, P. R. China

[3]Beijing National Laboratory for Molecular Sciences, CAS Key Laboratory of Organic Solids, Institute of Chemistry, Chinese Academy of Sciences, Beijing 100190, P. R. China

[4]College of Chemistry and Chemical Engineering, Central South University, Changsha 410083, P. R. China

[5]RIKEN Center for Emergent Matter Science, 2-1 Hirosawa, Wako, Saitama 351-0198, Japan

[6]School of Science and Engineering, the Chinese University of Hong Kong, Shenzhen 518172, P. R. China

Table of Contents

Part S1. General information

Material preparation: The compounds **SubPc-12H**, **SubPc-6F(β)** and **SubPc-12F** were synthesized according to the reported literatures[1-2].

Instruments and methods: NMR spectra were recorded on an Agilent 400-MR DD2 spectrometer. The ^{1}H NMR (400 MHz) chemical shifts were measured relative to $CDCl_3$ as the internal reference ($CDCl_3$: δ = 7.26 ppm). The ^{13}C NMR (100 MHz) chemical shifts were given using $CDCl_3$ as the internal standard (CDCl3: δ = 77.16 ppm). X-Ray single-crystal diffraction data were collected on an Agilent Technologies Gemini single-crystal diffractometer. Absorption spectra were obtained on a HITACHI U-2910 spectrometer. Cyclic voltammograms (CVs) were performed on LK2005A with a solution of tetrabutylammonium hexafluorophosphate (Bu_4NPF_6, 0.1 M) in DCM as electrolyte and ferrocene/ferrocenium (Fc/Fc^+) as standard. Three-electrode system (Ag/Ag^+, platinum wire and glassy carbon electrode as reference, counter, and work electrode, respectively) was used in the CV measurement. All potentials were corrected against Fc/Fc^+. CV was measured with a scan rate of 100 mV/s. Transmission electron microscopy (TEM) images were obtained by a transmission electron microscope (JEM-F200 from JEOL) operated at an accelerating voltage of 200 kV and selected area electron diffraction (SAED) was taken at an accelerating voltage of 200 kV. All the samples were prepared by directly drop-casting the micro-ribbon suspensions on a copper grid covered with a thin carbon support film. Ultraviolet photoemission spectroscopy (UPS) was conducted on a Kratos AXIS Ultra-DLD Photoelectron Spectrometer under an ultrahigh vacuum of about 10^{-8} Torr with an unfiltered He I gas discharge lamp source (21.22 eV). X-Ray diffraction (XRD) data were obtained using a Bruker D2 Phaser diffractometer with Cu-Kα radiation (λ = 1.5416 Å) at 30 kV and 10 mA. The sample was prepared as a standard powder mount, and the diffractogram was processed through the software JADE 6. Optical microscopies were collected on a BX53M system microscope from OLYMPUS.

Theoretical calculations: (1) The frontier molecular orbital distributions, reorganization energy, and electronic couplings were estimated at the DFT-B3LYP/6-31G(d,p) level by Gaussian 09 software[3] and visualized using Gaussview 5.0 software based on the single crystal structures. (2) The charge transfer integrals (t) were calculated at PW91PW91/6-31G(d,p) level based on the single crystal structures. (3) The Hirshfeld surface maps of SubPcs were performed by using the CrystalExplorer 17.5 program with inputting structure files in CIF format. All the Hirshfeld surfaces were generated using a standard (high) surface resolution. The 3D d_{norm} surface was mapped by using a fixed color scale of -0.1150 to 1.0069 Å. (4) The mobilities were calculated in the framework of the charge diffusion model in combination with the semi-classical Marcus theory.

Part S2. Single crystals of SubPcs

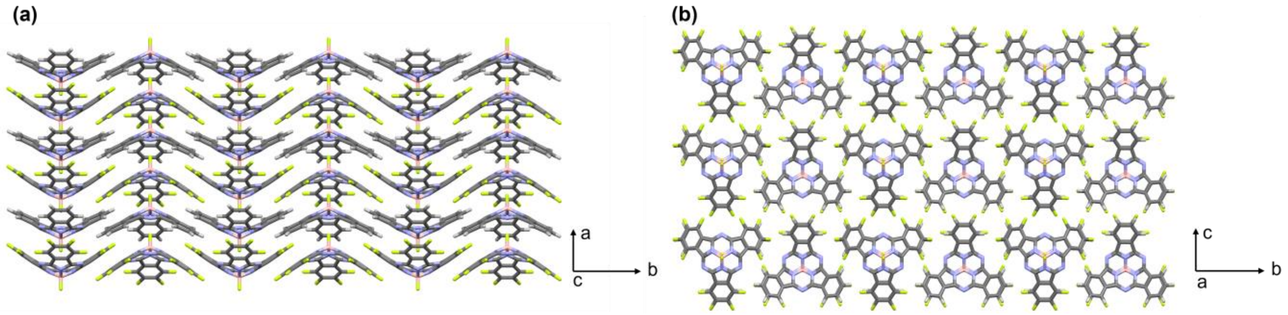

Figure S1. The a) side view and b) top view of **SubPc-12H-12F** cocrystal.

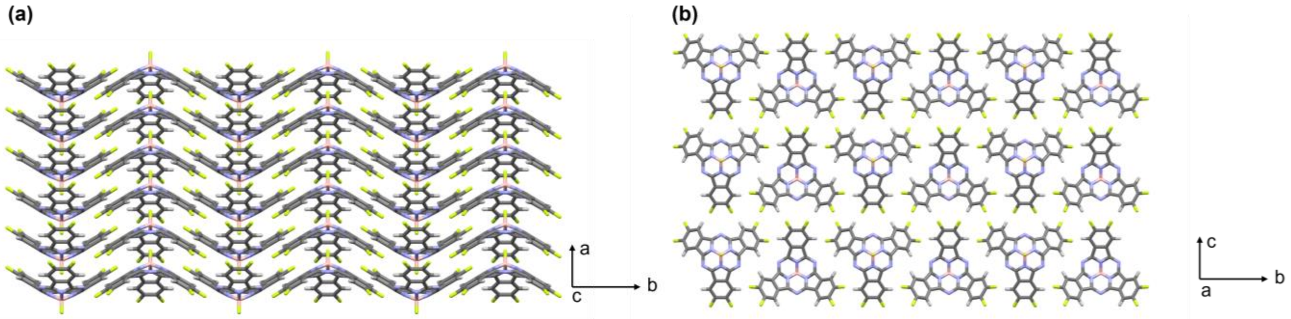

Figure S2. The a) side view and b) top view of **SubPc-6F(β)** single crystal.[4]

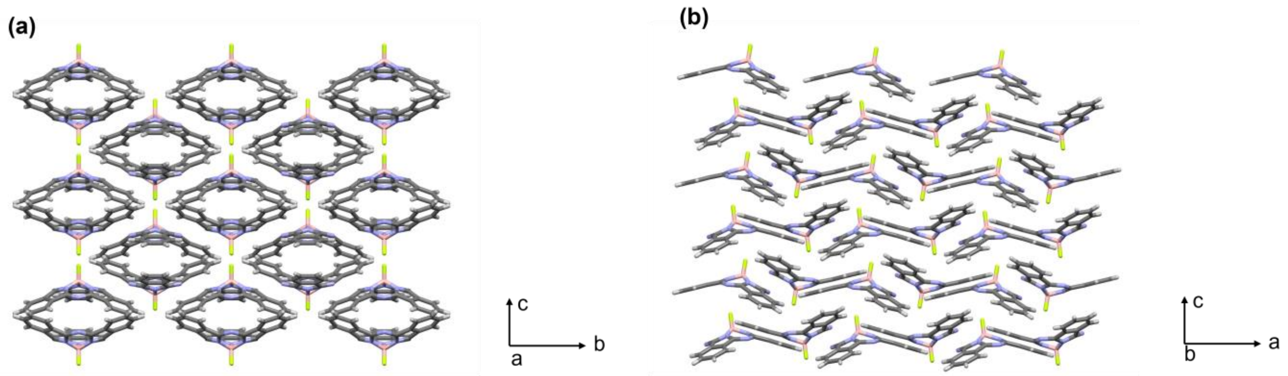

Figure S3. The view from a) *a*-axis and b) *b*-axis of **SubPc-12H** single crystal.[5]

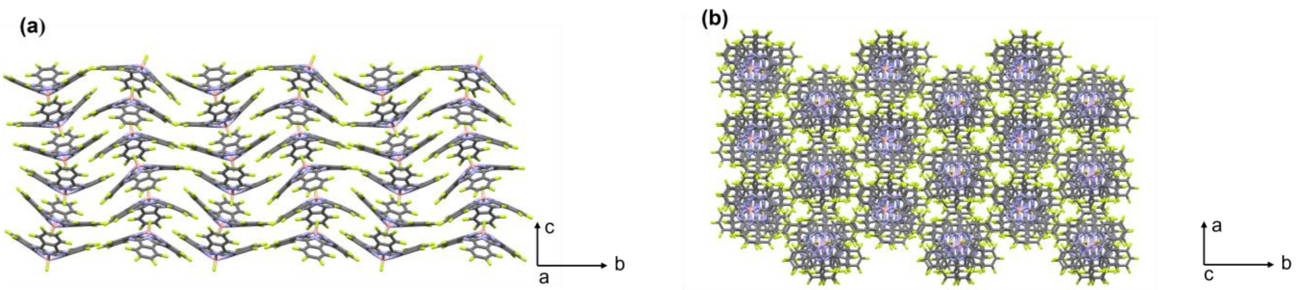

Figure S4. The a) side view and b) top view of **SubPc-12F** single crystal.[1]

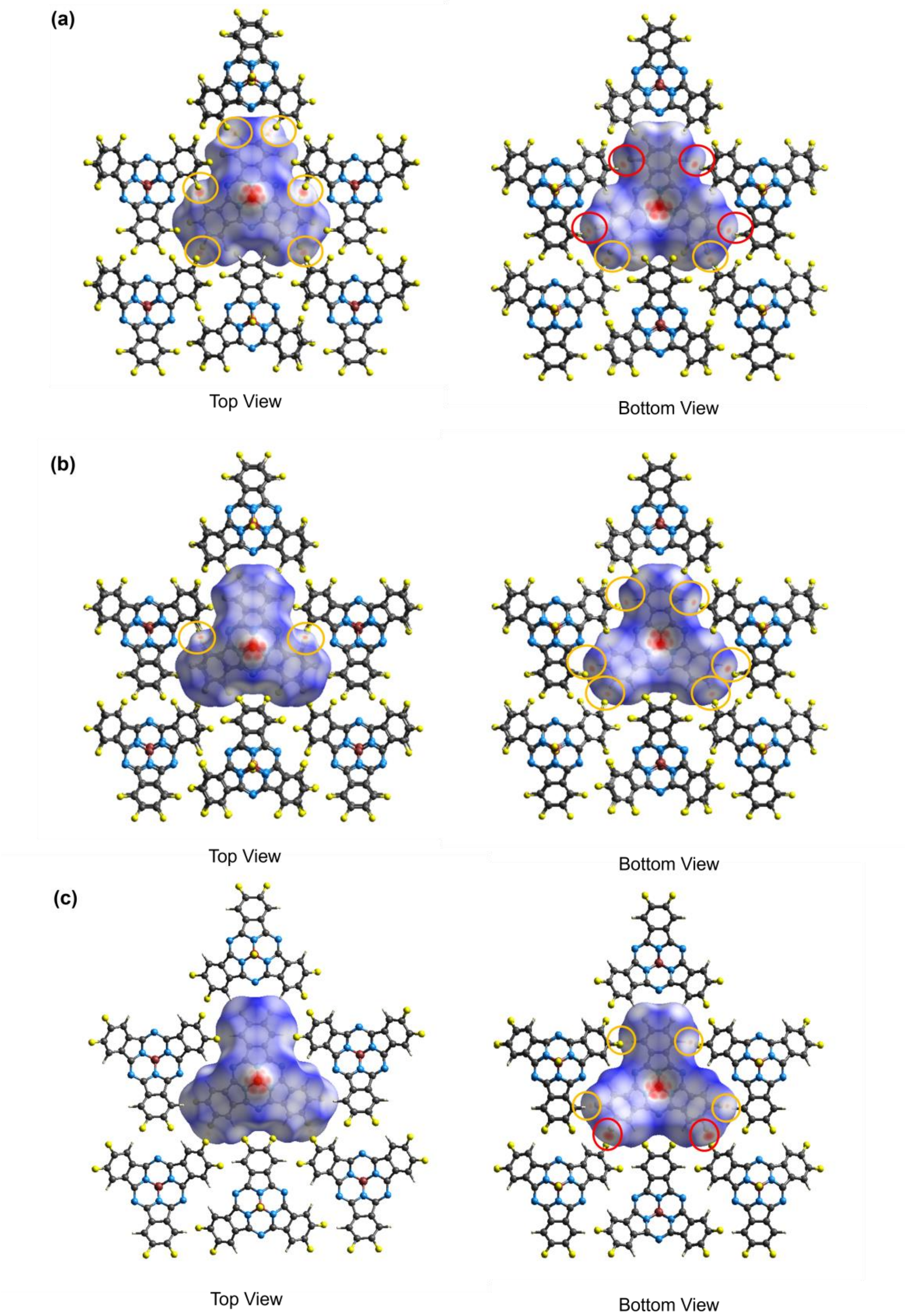

Figure S5. Hirshfeld surface maps of a, b) **SubPc-12H-12F** cocrystals and c) **SubPc-6F(β)** single crystals. a) **SubPc-12F** and b) **SubPc-12H** were selected as central molecules, respectively. In the Hirshfeld surface maps, the red parts indicate strong interactions, the yellow cycles represent F-H hydrogen and the red cycles represent F-F interaction.

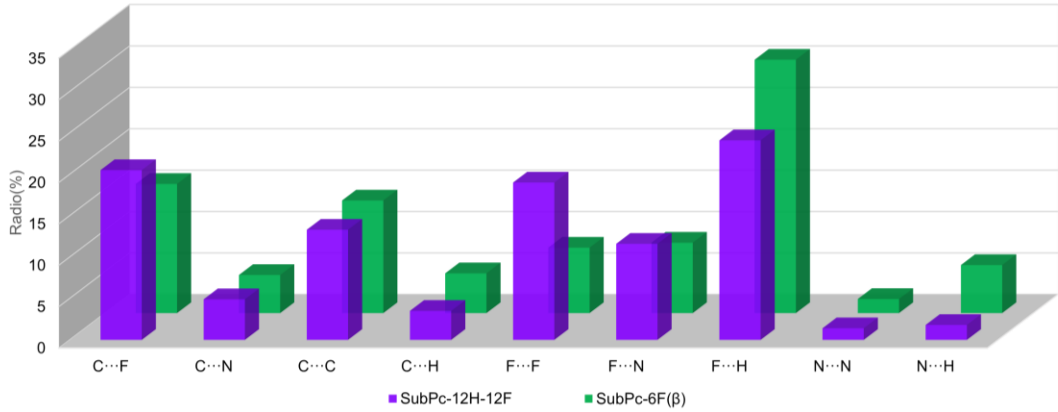

Figure S6. Relative contributions to the Hirshfeld d_{norm} surfaces for the various intermolecular contacts of **SubPc-12H-12F** and **SubPc-6F(β)**.

Table S1. Crystallographic data of **SubPc-12H-12F, SubPc-6F(β), SubPc-12H** and **SubPc-12F.**

Crystals	SubPc-12H-12F	SubPc-6F(β)	SubPc-12H	SubPc-12F
Crystal System	Monoclinic	Monoclinic	Orthorhombic	Orthorhombic
Crystal Symmetry	C_{2h}	C_{2h}	D_{2h}	D_2
Space Group	$P2_1/m$	$P2_1/m$	*P*nma	$P2_12_12_1$
a [Å]	8.6916(2)	4.3804(10)	12.1108(3)	11.5346(2)
b [Å]	19.7951(5)	19.3454(5)	14.3211(3)	22.1148(6)
c [Å]	11.5578(3)	12.1264(4)	10.3258(3)	26.3004(5)
α [°]	90	90	90	90
β [°]	95.196(7)	99.012(3)	90	90
γ [°]	90	90	90	90
V [$Å^3$]	1980.36(9)	1014.91(5)	1790.91	6708.85
Density [g cm^{-3}]	1.751	1.709	1.536	1.872
R [%]	4.57	4.34	3.82	3.71
R_w [%]	11.12	11.55	8.96	8.13
B-B Distance [Å]	4.35	4.38	-	-
π- π Distance[a] [Å]	3.50	3.50	-	-
Bowl Depth [Å]	2.79 (12H) 2.89 (12F)	2.97	2.48	2.71
Column Distance[b] [Å]	12.06	12.23	-	-

[a] The distances were the shortest among the three SubPc arms. [b]The distances were measured from the parallel columns.

Table S2. Crystal data and structure refinement for **SubPc-12H-12F**.

Compound	SubPc-12H-12F
Formula	$C_{24}BF_{13}N_6$, $C_{24}H_{12}BFN_6$
Molecular Weight	1044.32
Temperature [K]	100
Crystal System	Monoclinic
Crystal Symmetry	C_{2h}
Space Group	$P2_1/m$
a [Å]	8.6916(2)
b [Å]	19.7951(5)
c [Å]	11.5578(3)
α [°]	90
β [°]	95.196(7)
γ [°]	90
V [Å^3]	1980.36(9)
Z	2
Density [g cm^{-3}]	1.751
R [%]	4.57
R_w [%]	11.12
μ [mm^{-1}]	1.359
F [000]	1040
Crystal size [mm^3]	0.60 × 0.08 × 0.02
Radiation	CuKα (λ = 1.5418 Å)
2Θ range for data collection [°]	3.840 to 68.244
Index ranges	$-10 \leq h \leq 10$, $-22 \leq k \leq 23$, $-13 \leq l \leq 13$
Reflections collected	22091
Independent reflections	3723 [R_{int} = 0.0457, R_{sigma} = 0.0631]
Data/restraints/parameter	3723/0/355
Goodness-of-fit on F^2	1.012
Final R indexes [I>=2σ (I)]	R_1 = 0.0457, wR_2 = 0.1112
Final R indexes [all data]	R_1 = 0.0631, wR_2 = 0.1200
Largest diff. peak/hole [e Å^{-3}]	0.31/-0.26

Part S3. Photophysical and electrochemical properties of SubPcs

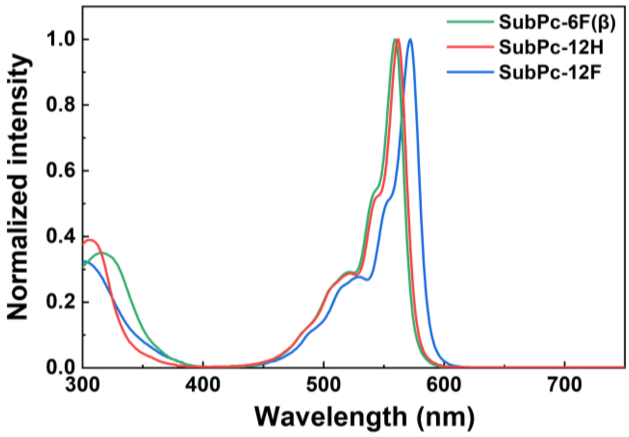

Figure S7. UV-vis absorption spectra of **SubPc-12H**, **SubPc-12F** and **SubPc-6F(β)** in dilute toluene (1.0×10^{-5} M).

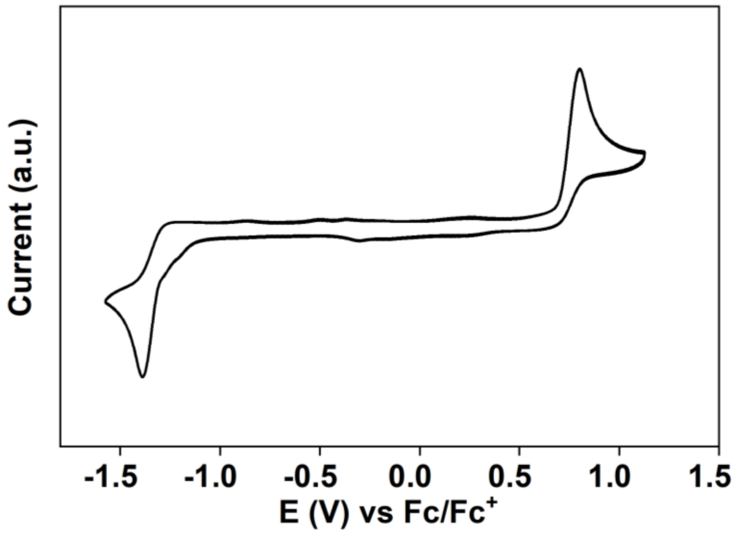

Figure S8. CV of **SubPc-6F(β)** in dry CH_2Cl_2 (1.0×10^{-3} M) containing 0.1 M Bu_4NPF_6.

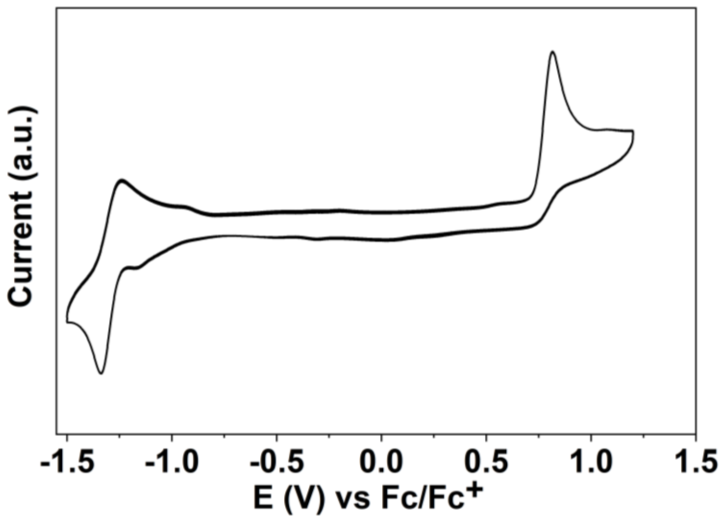

Figure S9. CV of **SubPc-12H** in dry CH_2Cl_2 (1.0×10^{-3} M) containing 0.1 M Bu_4NPF_6.

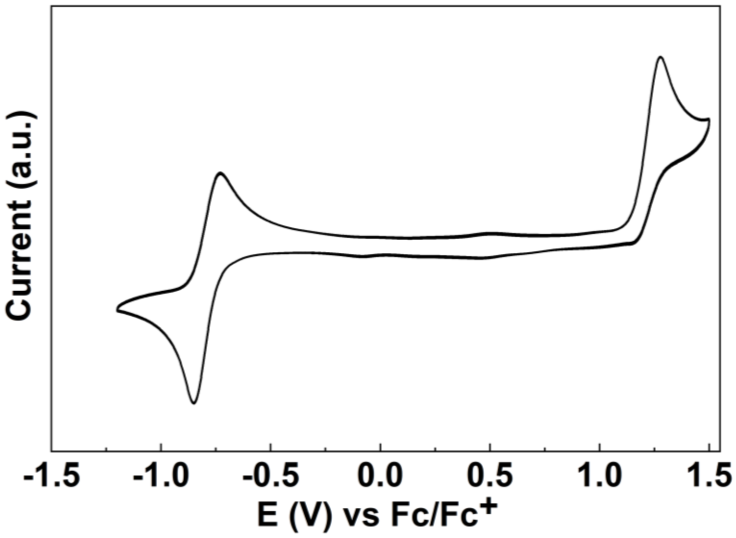

Figure S10. CV of **SubPc-12F** in dry CH_2Cl_2 (1.0×10^{-3} M) containing 0.1 M Bu_4NPF_6.

Table S3. Photophysical and electrochemical properties of SubPcs through UV/Vis absorption spectra in toluene and CVs**.**

Compounds	λ_{max}[a] [nm]	$E_g^{abs[b]}$ [eV]	HOMO[c] [eV]	LUMO[c] [eV]	$E_g^{CV[d]}$ [eV]
SubPc-12F	587	2.11	-5.71	-3.85	1.86
SubPc-6F(β)	574	2.16	-5.50	-3.49	2.01
SubPc-12H	576	2.15	-5.32	-3.33	1.99

[a] Absorption maxima in toluene (1.0×10^{-5} M). [b] The optical bandgaps were calculated according to $E_g = 1240/\lambda_{onset}$, where λ_{onset} is the onset value of the absorption spectrum in the long wavelength region. [c] From CVs measured in CH_2Cl_2 (1.0×10^{-3} M). The HOMO and LUMO energy levels are adjusted according to the redox half potential of Fc/Fc^+ and estimated according to the formula: E_{HOMO} (eV) = -(4.8 + E^{ox} - $E_{(Fc/Fc^+)}{}^{1/2}$), E_{LUMO} (eV) = -(4.8 + E^{red} - $E_{(Fc/Fc^+)}{}^{1/2}$). [d] Estimated according to the formula: E_g (eV) = E_{LUMO} - E_{HOMO}.

Part S4. OFET device fabrication and evaluation procedure

OFET device fabrication process: The surface of the substrates with 300-nm-thick thermally oxidized SiO_2 on doped Si was cleaned orderly with deionized water, piranha solution (H_2SO_4/H_2O_2 = 7:3), deionized water, isopropyl alcohol, and finally were blown dry with high-purity nitrogen gas. Octadecyltrichlorosilane (OTS) modifying SiO_2/Si wafers was carried out with the vapor-deposition method: the cleaned wafers were dried under vacuum at 90 ℃ for 0.5 h to eliminate the moisture. When the temperature decreased to 70 ℃, a small drop of OTS was dropped onto the wafers. Subsequently, this system was heated to 120 ℃ for 2 h under vacuum. OTS modified SiO_2/Si wafers used here were cleaned with n-hexane, chloroform, and isopropyl alcohol in sequence, and finally were blown dry with high-purity nitrogen gas. The organic crystal was deposited on the OTS-treated substrates by a PVT process, gold source and drain contacts (60 nm in thickness) were deposited on the organic layer by vacuum evaporation, affording a bottom-gate top-contact configuration.

OFET performance evaluation: Transfer and output characteristics of OFETs were collected using a semiconductor parameter analyzer (Keithley BT1500A). Field-effect mobility values (μ_{sat}) were estimated from the saturation regime using the following equation:

$$-I_D = (WC_i/2L)\ \mu_{sat}\ (V_G - V_{th})^2$$

C_i is the capacitance of the gate insulator, V_{th} is the threshold voltage, and L and W are the length and width of the channel, respectively.[6]

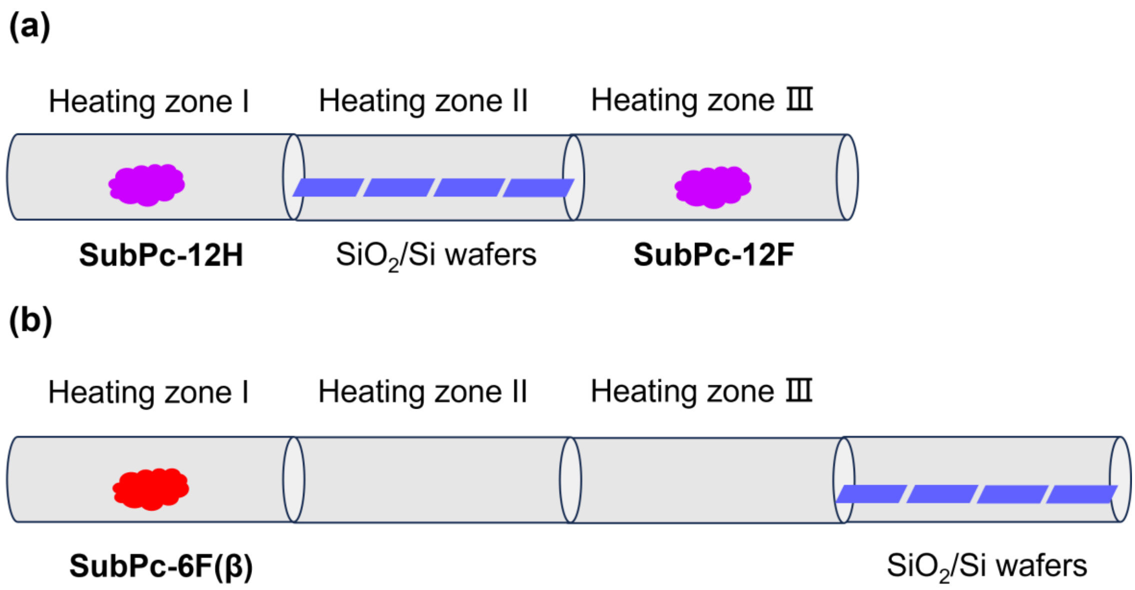

Figure S11. The schematic of the PVT process to prepare a) **SubPc-12H-12F** and b) **SubPc-6F(β)** crystals.

Table S4. Temperature conditions of PVT process.

Materials	Heating zone I (°C)	Heating zone II (°C)	Heating zone III (°C)
SubPc-12H-12F	215 (**SubPc-12H**)	150	205 (**SubPc-12F**)
SubPc-6F(β)	200	150	100

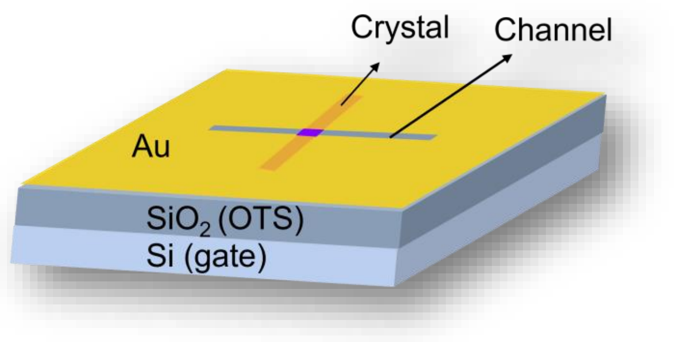

Figure S12. The schematic device structure of OFETs with bottom-gate top-contact configuration.

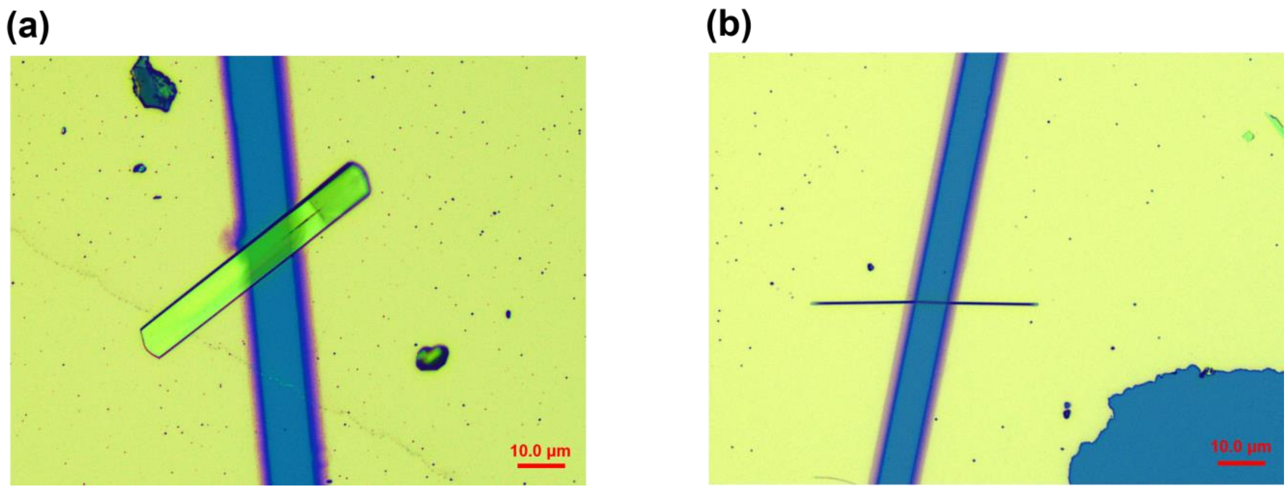

Figure S13. The representative optical microscopy images of a) **SubPc-12H-12F** cocrystal and b) **SubPc-6F(β)** single crystal attached with Au electrode.

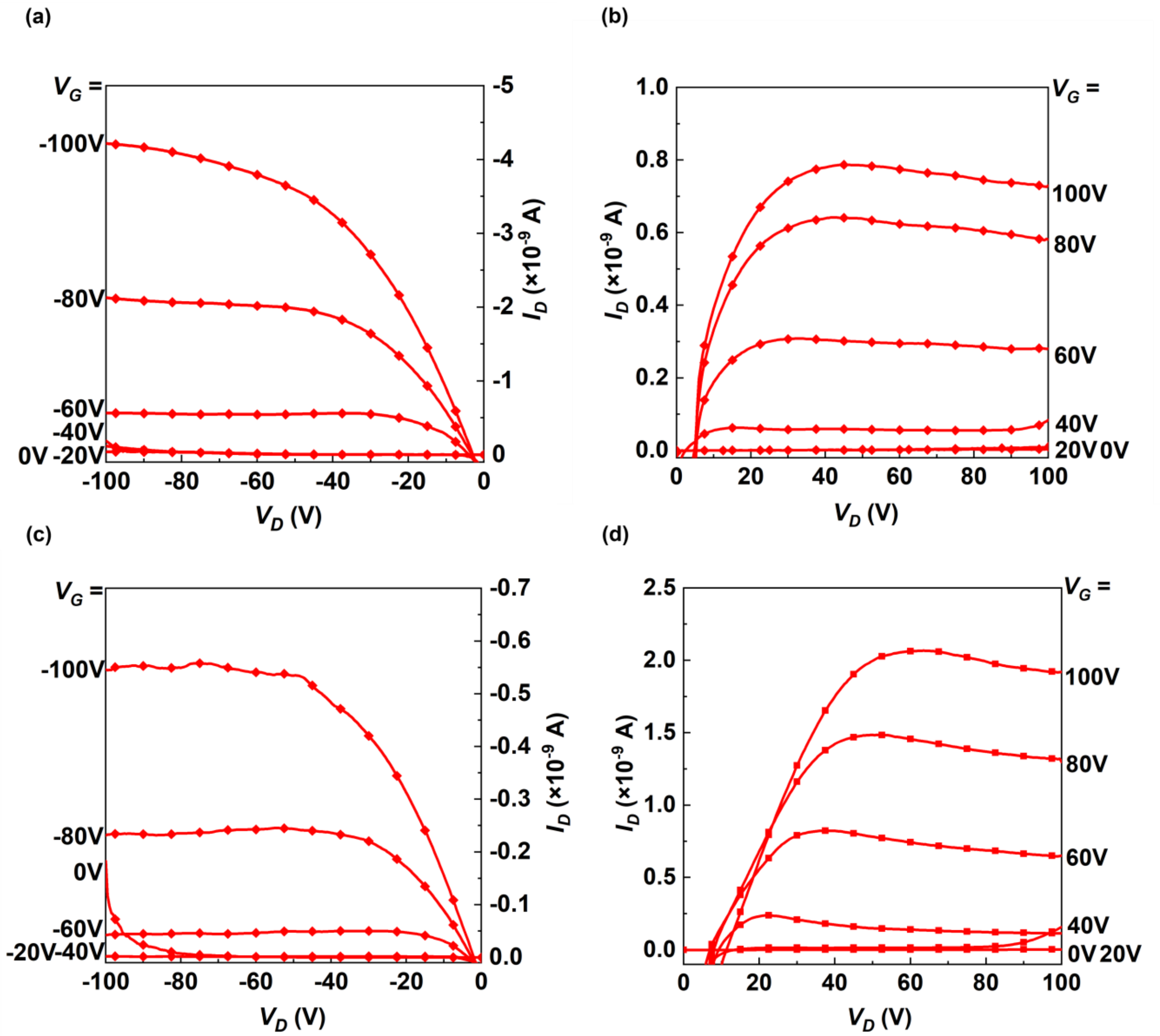

Figure S14. The representative output curves of a, c) hole and b, d) electron transport with a, b) **SubPc-12H-12F** and c, d) **SubPc-6F(β)** in OFET devices.

Part S5. Theoretical calculation

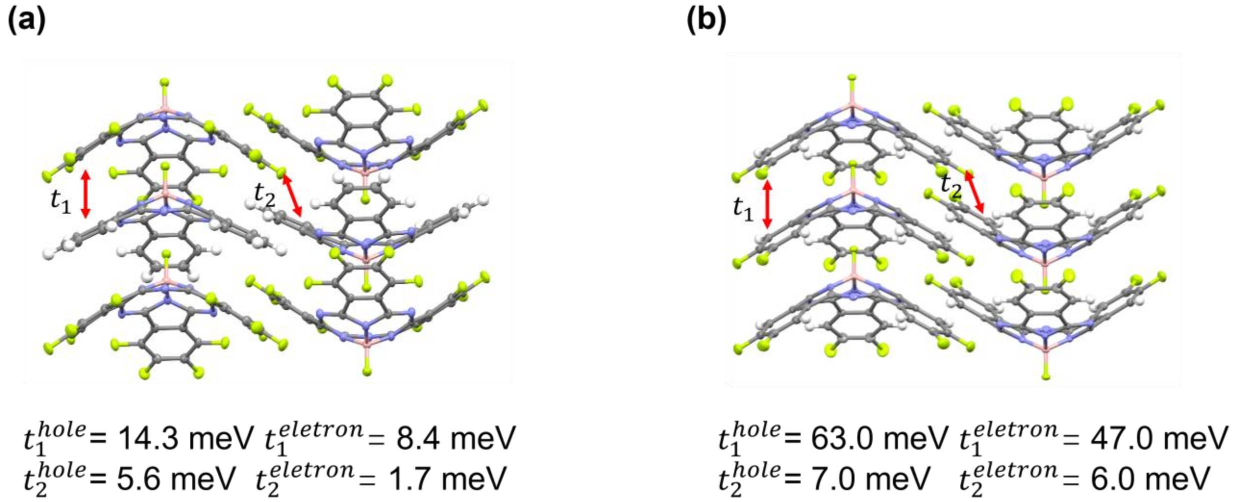

Figure S15. The transfer integrals of a) **SubPc-12H-12F** and b) **SubPc-6F(β)**.

Table S5. Reorganization energy.

Materials	λ_e [meV]	λ_h [meV]
SubPc-12H-12F	310	146
SubPc-6F(β)	300	120

Table S6. Mobility [cm^2 V^{-1} s^{-1}] evaluations along each axis and overall mobilities of crystals.

Materials	Electron Mobility			μ_e	$\mu_{e, eff}$[a]
	a-axis	*b*-axis	*c*-axis		
SubPc-12H-12F	0.0427	0.106	0.0306	0.0593	0.0856
SubPc-6F(β)	0.2142	0.0545	0.0114	0.0765	-
Materials	**Hole Mobility**			μ_h	$\mu_{h, eff}$[a]
	a-axis	*b*-axis	*c*-axis		
SubPc-12H-12F	0.353	0.597	0.643	0.5280	0.9266
SubPc-6F(β)	0.0208	0.0507	0.544	0.8876	-

[a] The mobilities were evaluated with super-exchange couplings.

Part S6. NMR spectra

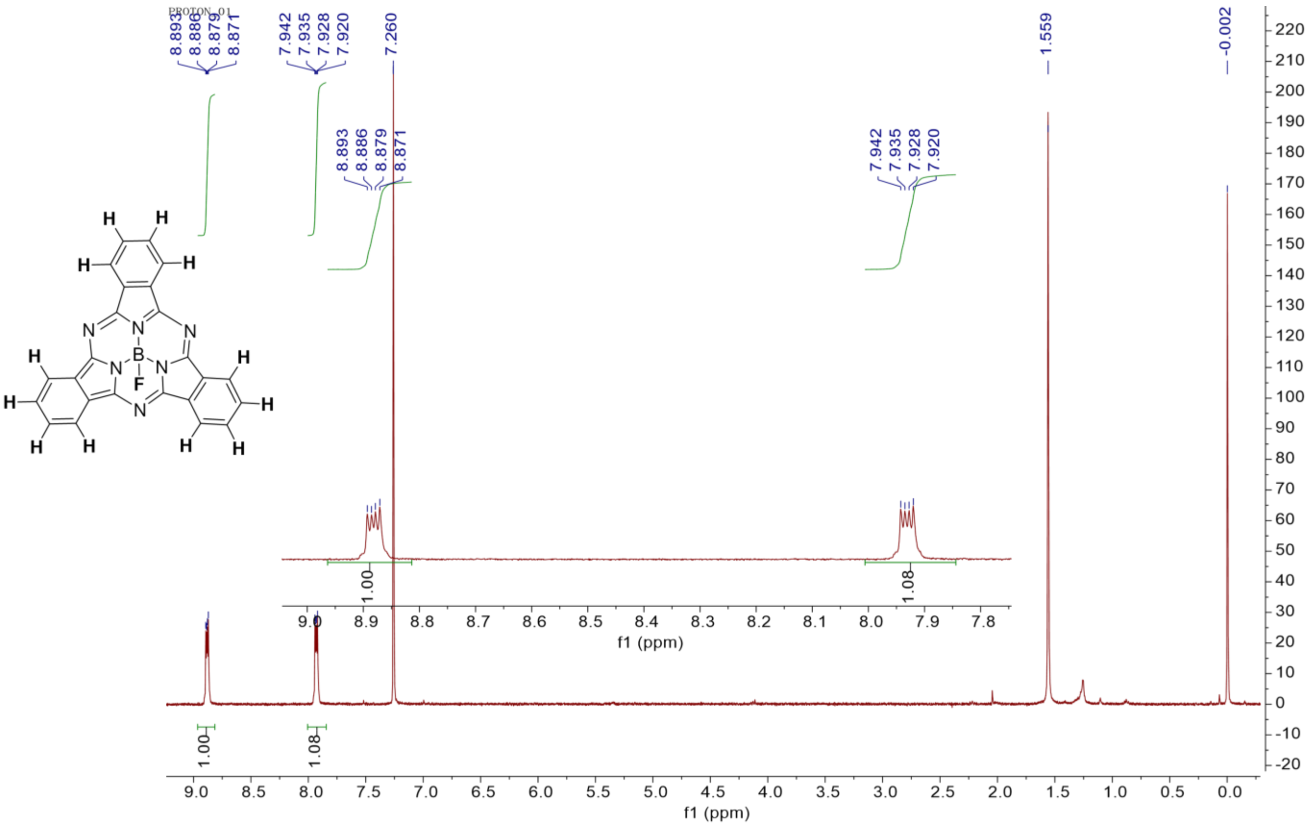

Figure S16. The ^{1}H NMR spectra of **SubPc-12H**.

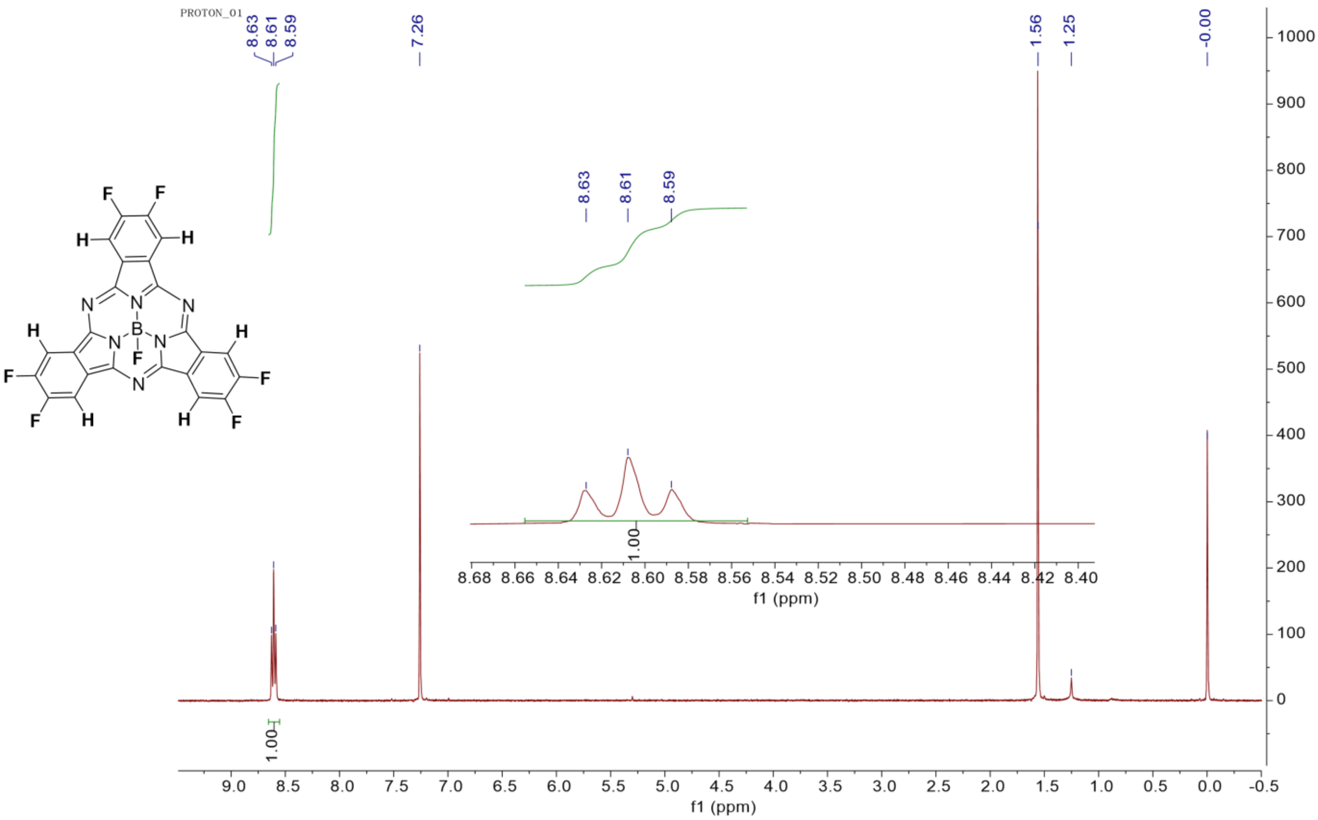

Figure S17. The ^{1}H NMR spectra of **SubPc-6F(β)**.

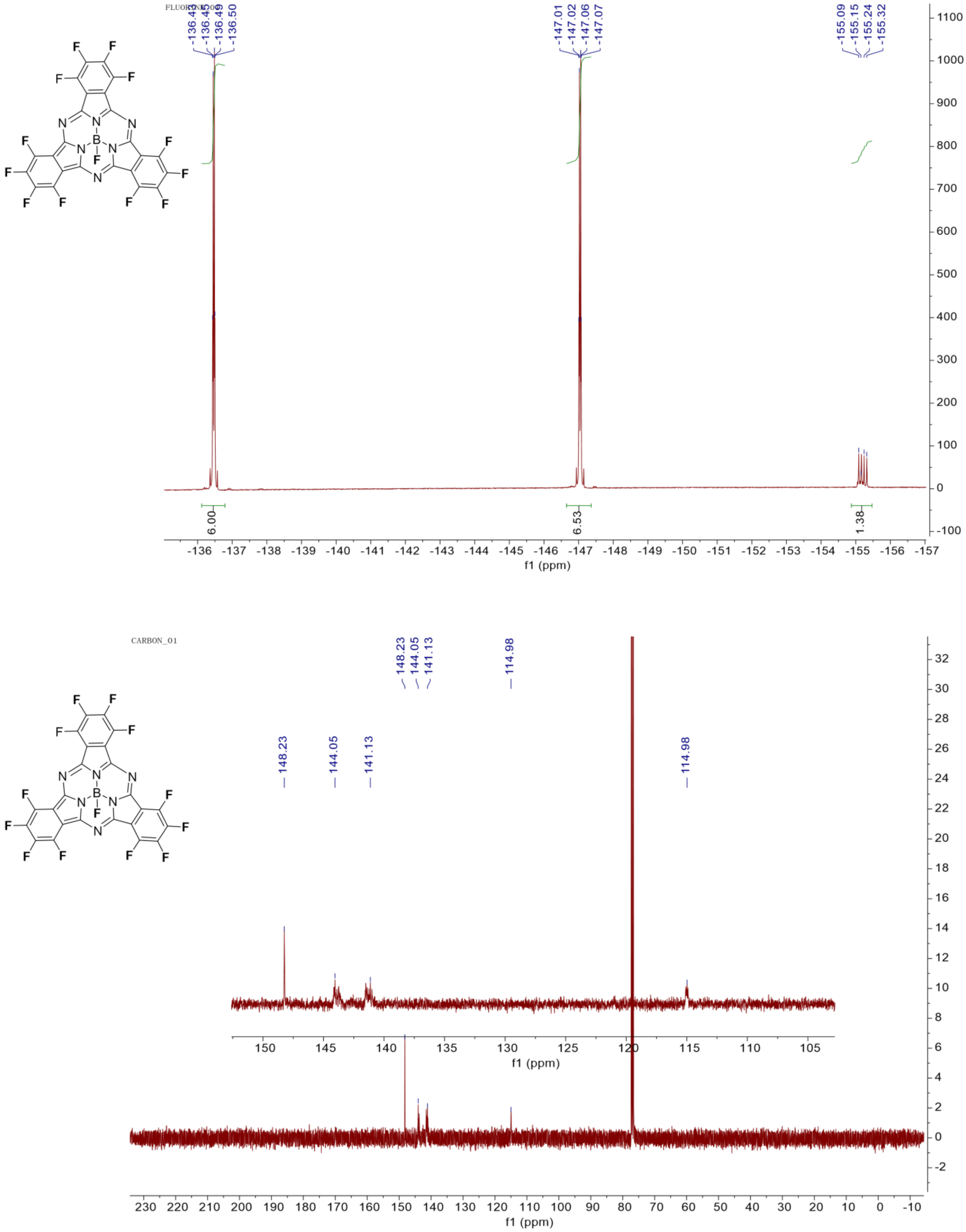

Figure S18. The ^{19}F NMR (up) and ^{13}C NMR (down) spectra of **SubPc-12F**.

Part S7. References

[1] E. Bukuroshi, J. Vestfrid, Z. Gross, T. P. Bender, *New J. Chem.* **2019**, *43*, 16730.

[2] J. Guilleme, D. Gonzlez-Rodrguez, T. Torres, *Angew. Chem. Int. Ed.* **2011**, *50*, 3506.

[3] M. J. Frisch, G. W. Trucks, H. B. Schlegel, G. E. Scuseria, M. A. Robb, J. R. Cheeseman, G. Scalmani, V. Barone, B. Mennucci, G. A. Petersson, H. Nakatsuji, M. Caricato, X. Li, H. P. Hratchian, A. F. Izmaylov, J. Bloino, G. Zheng, J. L. Sonnenberg, M. Hada, M. Ehara, K. Toyota, R. Fukuda, J. Hasegawa, M. Ishida, T. Nakajima, Y. Honda, O. Kitao, H. Nakai, T. Vreven, J. A. Jr. Montgomery, J. E. Peralta, F. Ogliaro, M. Bearpark, J. J. Heyd, E. Brothers, K. N. Kudin, V. N. Staroverov, R. Kobayashi, J. Normand, K. Raghavachari, A. Rendell, J. C. Burant, S. S. Iyengar, J. Tomasi, M. Cossi, N. Rega, N. J. Millam, M. Klene, J. E. Knox, J. B. Cross, V. Bakken, C. Adamo, J. Jaramillo, R. Gomperts, R. E. Stratmann, O. Yazyev, A. J. Austin, R. Cammi, C. Pomelli, J. W. Ochterski, R. L. Martin, K. Morokuma, V. G. Zakrzewski, G. A. Voth, P. Salvador, J. J. Dannenberg, S. Dapprich, A. D. Daniels, Ö. Farkas, J. B. Foresman, J. V. Ortiz, J. Cioslowski, D. J. Fox, Gaussian 09, Revision D.01, Gaussian, Inc., Wallingford CT, **2009**.

[4] C. Zhang, Y. Guo, D. He, J. Komiya, G. Watanabe, T. Ogaki, C. Wang, A. Nihonyanagi, H. Inuzuka, H. Gong, Y. Yi, K. Takimiya, D. Hashizume, D. Miyajima, *Angew. Chem. Int. Ed.* **2021**, *60*, 3261.

[5] M. V. Fulford, D. Jaidka, A. S. Paton, G. E. Morse, E. R. L. Brisson, A. J. Lough, T. P. Bender, *J. Chem. Eng.* **2012**, *57*, 2756.

[6] H. Chen, W. Zhang, M. Li, G. He, X. Guo, *Chem. Rev.* **2020**, *120*, 2879.